LAWRENCE
LIVERMORE
NATIONAL
LABORATORY

LLNL-JRNL-654156

Inferring Aftershock Sequence Properties and Tectonic Structure Using Empirical Signal Detectors

W. N. Junek, T. Kvaerna, M. Pirli, J. Schweitzer, D. B. Harris, D. A. Dodge, M. T. Woods

May 8, 2014

Pure and Applied Geophysics

Disclaimer

This document was prepared as an account of work sponsored by an agency of the United States government. Neither the United States government nor Lawrence Livermore National Security, LLC, nor any of their employees makes any warranty, expressed or implied, or assumes any legal liability or responsibility for the accuracy, completeness, or usefulness of any information, apparatus, product, or process disclosed, or represents that its use would not infringe privately owned rights. Reference herein to any specific commercial product, process, or service by trade name, trademark, manufacturer, or otherwise does not necessarily constitute or imply its endorsement, recommendation, or favoring by the United States government or Lawrence Livermore National Security, LLC. The views and opinions of authors expressed herein do not necessarily state or reflect those of the United States government or Lawrence Livermore National Security, LLC, and shall not be used for advertising or product endorsement purposes.

Noname manuscript No.
(will be inserted by the editor)

Inferring Aftershock Sequence Properties and Tectonic Structure Using Empirical Signal Detectors

William N. Junek · Tormod Kvaerna · Myrto Pirli · Johannes Schweitzer · David B. Harris · Douglas A. Dodge · Mark T. Woods

Received: date / Accepted: date

Abstract Seismotectonic studies of the 2008 Storfjorden aftershock sequence were limited to data acquired by the permanent, but sparse, regional seismic network in the Svalbard archipelago. Storfjorden's remote location and harsh polar environment inhibited the deployment of temporary seismometers that would have improved observations of sequence events. The lack of good station coverage prevented the detection and computation of hypocenter locations of many low magnitude events (mb $<$ 2.5) in the NORSAR analyst reviewed bulletin. As a result, the fine structure of the sequence's space-time distribution was not captured. In this study, an autonomous event detection and clustering framework is employed to build a more complete catalog of Storfjorden events using data from the Spitsbergen (SPITS) array. The new catalog allows the spatiotemporal distribution of seismicity within the fjord to be studied in greater detail. Information regarding the location of active event clusters provides a means of inferring the tectonic structure within the fault zone. The distribution of active clusters and moment tensor solutions for the Storfjorden sequence suggests there are at least two different structures within the fjord: a NE-SW trending linear feature with oblique-normal to strike-slip faulting and E-W trending normal faults.

W. N. Junek · M. T. Woods
Air Force Technical Applications Center
Patrick Air Force Base Florida
E-mail: william.junek@us.af.mil

T. Kvaerna · M. Pirli · J. Schweitzer
NORSAR
Kjeller, Norway

D. A. Dodge
Lawrence Livermore National Laboratory
Livermore, California, USA

D. B. Harris
Deschutes Signal Processing
Maupin, Oregon, USA

Keywords Correlation Detectors · Subspace Detectors · Aftershock Sequence · Tectonics · Seismicity

1 Introduction

Aftershock sequences are typically studied using a dense network of seismometers consisting of existing instruments and temporary stations whose deployment is optimized for studying a particular sequence. This arrangement provides seismologists with the means to detect low magnitude events, compute more accurate hypocenter locations, and generate relative relocation catalogs. Results provide insight into the seismotectonics of the region and are useful for seismic hazard studies. The remote location of some aftershock sequences makes the deployment of temporary sensors impractical. Factors inhibiting such deployments include: harsh environmental conditions (e.g., polar climate, glaciation, off-shore location), cost, and lack of physical infrastructure (e.g., manpower, electricity). In these situations, seismologists are forced to use existing resources to study the sequence.

The 2008 Storfjorden aftershock sequence occurred off Spitsbergen's southeast coastline. Its remote location, polar environment, off-shore location, and lack of physical infrastructure limited the deployment of temporary seismometers. As a result, only the permanent stations in the region were used to study its evolution. The sequence was triggered by an M_w 6.2 earthquake that occurred off Svalbard's southeastern coast on February 21, 2008. Over the following five years, it generated thousands of aftershocks; sixteen have exceeded M_w 4.0. Figure 1 shows the locations (in green) of sequence events published in NORSAR's analyst reviewed regional bulletin. Investigations of the regional seismotectonics concluded the source of the sequence was not related to the nearby Billefjorden fault zone (BFZ). Instead, its source is most likely tied to the Tertiary Shear Zone (TSZ)

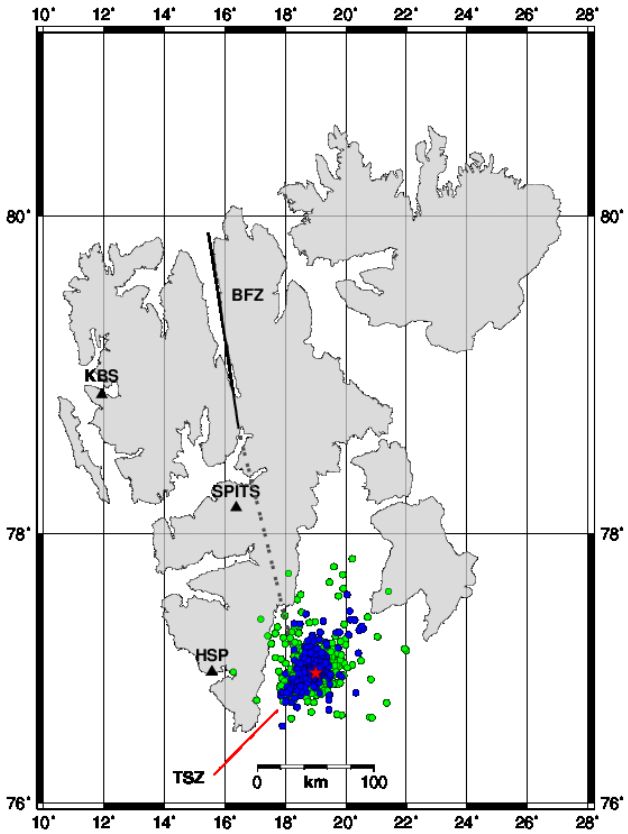

Fig. 1: The Storfjorden aftershock sequence occurred off Spitsbergen's southeast coast. Events shown in green represent the NORSAR analyst reviewed catalog between 21 February 2008 and 20 April 2012. The red star shows the location of the main shock and blue dots represent the relative relocation catalog (Pirli et al., 2013). The red line shows the location of the shear zone suggested by Bergh & Grogan (2003), believed to be related with the Storfjorden sequence (Pirli et al., 2013). Black triangles show the locations of some of the permanent seismic stations on Spitsbergen. The solid black line shows the location of the Billefjorden fault zone and the black dotted line is one of the proposed hypothetical extensions into the fjord.

shown in red in Figure 1. This conclusion is supported by the orientation of the relative relocation catalog, shown in blue in Figure 1, and the orientations of focal mechanisms for numerous sequence events (Pirli et al., 2013; Junek et al., 2014). These studies were largely based on the analysis of manually reviewed events. However, the number of events in the NORSAR analyst reviewed bulletin represent a small fraction of the total number of events produced by the sequence.

In this study, an autonomous event detection and clustering framework is used to expand the Storfjorden sequence dataset. The framework automatically spawns new or updates an existing empirical signal detector (ESD) pool upon the detection of a new signal. It groups detections based on waveform similarity and stores detection association information in a relational database. This process allows for the detection of low magnitude events originating from common source types and locations to be grouped into families and tracked over the course of the sequence. The expanded dataset is used to infer information about the tectonic structure within the fjord and to examine the sequence's spatiotemporal properties.

2 Signal and Data Processing Methods

An ESD is a generic term that encapsulates many types of multichannel matched filters, which include: array-based correlation, array signal subspace, and single channel correlation detectors. Numerous studies have demonstrated the power of ESDs for detecting seismic events and measuring their similarity (Harris, 2006; Gibbons & Ringdal, 2006; Schaff & Waldhauser, 2010; Slinkard et al., 2013). They are capable of detecting low signal-to-noise ratio (SNR) signals that originate from a common source type and location, which are difficult for conventional power detectors (e.g., STA/LTA) to identify.

The framework is a java based application that was developed as a collaborative effort between Lawrence Livermore National Laboratory and NORSAR. A block diagram highlighting the framework's core functionality is shown in Figure 2, and a complete description of an early version of the system is provided in Harris & Dodge (2011). The framework uses power (STA/LTA) detectors operating on array beams to detect events with new waveform patterns, and automatically spawns correlation detectors to search for additional occurrences of events with those patterns. The framework maintains a pool of such empirically-derived correlation detectors, which may be updated upon the detection of new signals approximately matching the patterns. It groups signal detections based on waveform similarity and stores event affiliation information in a relational database. All framework detections are tagged with an identification number (detector ID) that represents new or previously observed signal types. The database can be mined to study the various aspects of the sequence. For example, detector IDs can be grouped and associated detections counted to identify event clusters. Processing can be initiated using stored detectors and reconfigured to use a lower detection threshold. This dynamic reconfiguration allows waveform templates built during later periods of the sequence to be applied to earlier portions of the sequence. Typically this reconfiguration results in the detection of many low SNR signals that were missed in the initial pass through the data.

Event size is estimated using a relative magnitude (mb_{rel}) relationship that scales newly detected events against a user defined master event (Junek et al., 2008). The relative scal-

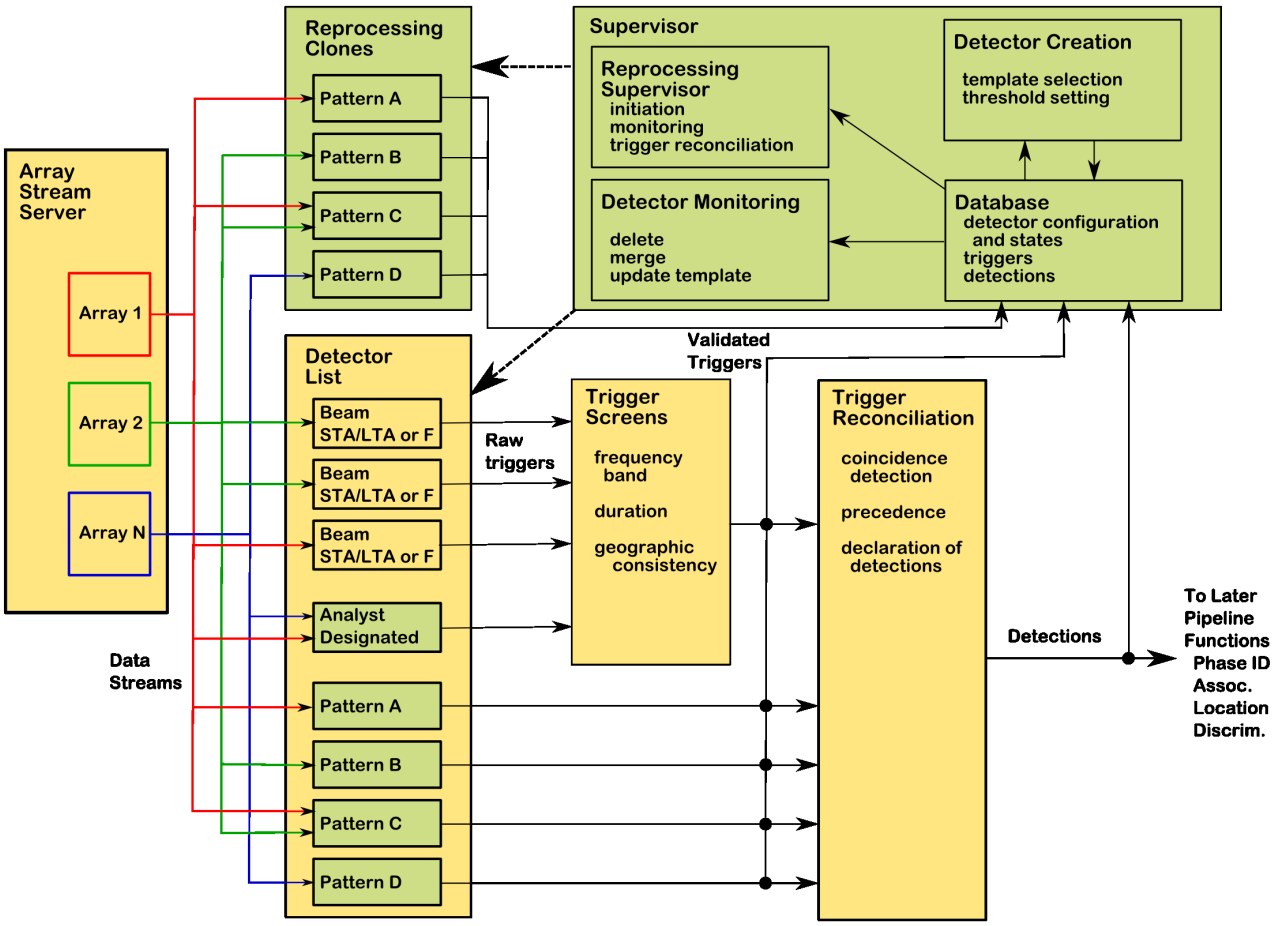

Fig. 2: Autonomous seismic signal detection and event grouping framework block diagram, where yellow blocks represent components found in typical seismic data processing pipelines and green blocks show infrastructure reqiured to support the framework (Harris & Dodge, 2011).

ing relationship used in this study is defined as

$$mb_{rel} = mb_r + log_{10}\left(\frac{A_n}{A_r}\right) \tag{1}$$

where mb_r is the reference event bodywave magnitude, A_r is the peak amplitude of the reference event seismogram, and A_n is the peak amplitude of the new event seismogram. Amplitude measurements for reference and newly detected signals are made on P-waves filtered in the same passband. The reference magnitude is adjusted based on the value of the log amplitude ratio. Since all of the events under consideration are originating from a small area, no distance correction is introduced. The relative magnitude scale allows bodywave magnitudes to be calculated for all SPITS ESD detections. Relative magnitude estimates are used to produce a cumulative frequency magnitude distribution (FMD) that quantifies the minimum detection threshold for SPITS relative to the Storfjorden region. The analyst reviewed and framework generated catalogs can be compared to quantify the framework's performance.

Determination of the catalog completeness magnitude (M_c) is conducted using the method outlined in Wiemer & Wyss (2000). This technique compares the linear sections of the observed and modeled FMD between the maximum magnitude and an assumed M_c. The goodness of fit between the modeled and observed FMDs is assessed using

$$R(a, b, M_i) = 100 - \frac{\sum_{M_i}^{M_{max}} |B_i - S|}{\sum_i B_i} 100 \tag{2}$$

where R is the goodness of fit, a and b are the Gutenberg-Richter relationship coefficients, M_i is the completeness magnitude being tested, and B and S are the observed and predicted portions of the distribution for each magnitude bin (Wiemer & Wyss, 2000; Gutenberg & Richter, 1944). The Gutenberg-Richter coefficients are determined using a least-squares regression before the initiation of the M_c estimation routine. This is an iterative process that tests the validity

Table 1: Processing parameters employed by detection framework for Storfjorden sequence using SPITS data.

Parameter	Value	Description
$Filter$	Bandpass	3 pole Butterworth filter
F_{lo}	2.0 Hz	Low frequency corner
F_{hi}	8.0 Hz	High frequency corner
TL_{min}	20.0 s	Minimum template length
TL_{max}	33.0 s	Maximum template length
$Azimuth$	155.0 deg	Detection beam azimuth
$Velocity$	5.5 km/s	Beam velocity
Az_{tol}	$\pm$ 20.0 deg	Azimuth tolerance
Vel_{tol}	$\pm$ 1.0 km/s	Velocity tolerance
T_{AP}	20.0 (4.5 linear)	Array power detector threshold
T_{ESD}	0.2 (0.45 linear)	ESD detection threshold

of many M_c values. Here we chose the M_i value with the largest R as the catalog M_c.

3 Discussion of Results

3.1 Processing Configuration

The detection framework was used to process 7 vertical, broadband, elements of the SPITS array between February 21, 2008 and April 20, 2012. Processing parameter values and descriptions are listed in Table 1. The array power detector threshold was set high so only high quality signals are used as ESD templates. Since our ESDs have a large time bandwidth product and use multiple channels of the array, T_{ESD} was set to 0.2. This value was selected empirically after visual inspection of the correlation trace noise floor. Frequency-Wavenumber (FK) screening was used to remove detections outside of Storfjorden. Signal duration was used as an additional screening metric to discard unrelated detections. Valid detections had durations that fell between TL_{min} and TL_{max}.

3.2 Detection Statistics

The total number of detections and event clusters produced by the detection framework are listed in Table 2. Here FK screening occurs during post processing via an application that runs outside the detection framework. As a result, all array power detections are used to spawn new correlation detectors regardless of their slowness vector. Since the SPITS array observes seismicity from numerous local, regional, and teleseismic sources, a large number of detectors are formed from sources outside of Storfjorden.

Figures 3 and 4 show FK measurements for all detections made over the four and half year processing interval, where black dots fall within the azimuth, velocity, and FK power (see Appendix A) constraints listed in Table 1 and red dots do not. The time series plot shows the ESDs are identifying events arriving on numerous azimuth and slowness vectors. The azimuth plot shows detections are typically made along back azimuths of 330, 220, and 150 degrees. The polar plot shows numerous sources of repeating seismicity near the station. Sources of repeating seismicity include mining activity, ice quakes, local earthquakes, Mid-Atlantic Ridge earthquakes, and Storfjorden events (shown in black). The large number of off target detections highlights the need for post detection azimuth and slowness screening for automatically generated ESDs.

Table 2: Framework detection results, where Y denotes the application of FK screening and N its absences. The detection field denotes the number of detector triggers and the Event Type field represents the number of unique ESDs deployed by the system in parallel.

Parameter	FK Screening	Results
Detections	Y	15911
	N	76688
Event Type	Y	2509
	N	5072

Table 3: FK measurements for events shown in Figures 5(a) - 5(d)

Example	Azimuth (deg)	Velocity (km/s)
Event 1	152.89	5.53
Event 2	122.13	9.29

Table 2 shows the number of framework detections and unique ESDs deployed in parallel by the system over the course of the sequence. Approximately 80% of the detections and 51% of the ESDs were rejected after the screening metrics were applied. Examples of valid and invalid event detections with their corresponding FK spectra are shown in Figures 5(a) - 5(d). Example one is a valid detection whose wavefront arrives at the station on the expected azimuth and slowness vector. Example two is also a valid signal detection whose wavefront arrives at the station on an azimuth and slowness vector that is inconsistent with Storfjorden. As a result, event one is associated to the Storfjorden sequence, while event 2 is rejected and not considered in subsequent analysis.

Figures 6, 7, and 8 show the magnitude distributions and M_c estimates for the framework and NORSAR catalogs. The histogram of framework detections almost completely eclipses the analyst reviewed bulletin. Cumulative FMDs show the two distributions have similar b values and highlights detection threshold differences between the two catalogs. M_c estimates for the framework and NORSAR catalogs with the largest R values are 0.8 and 2.1. The difference in M_c estimates shows the framework is providing a 1.3 magnitude unit improvement in detection capability for Storfjorden events observed by SPITS.

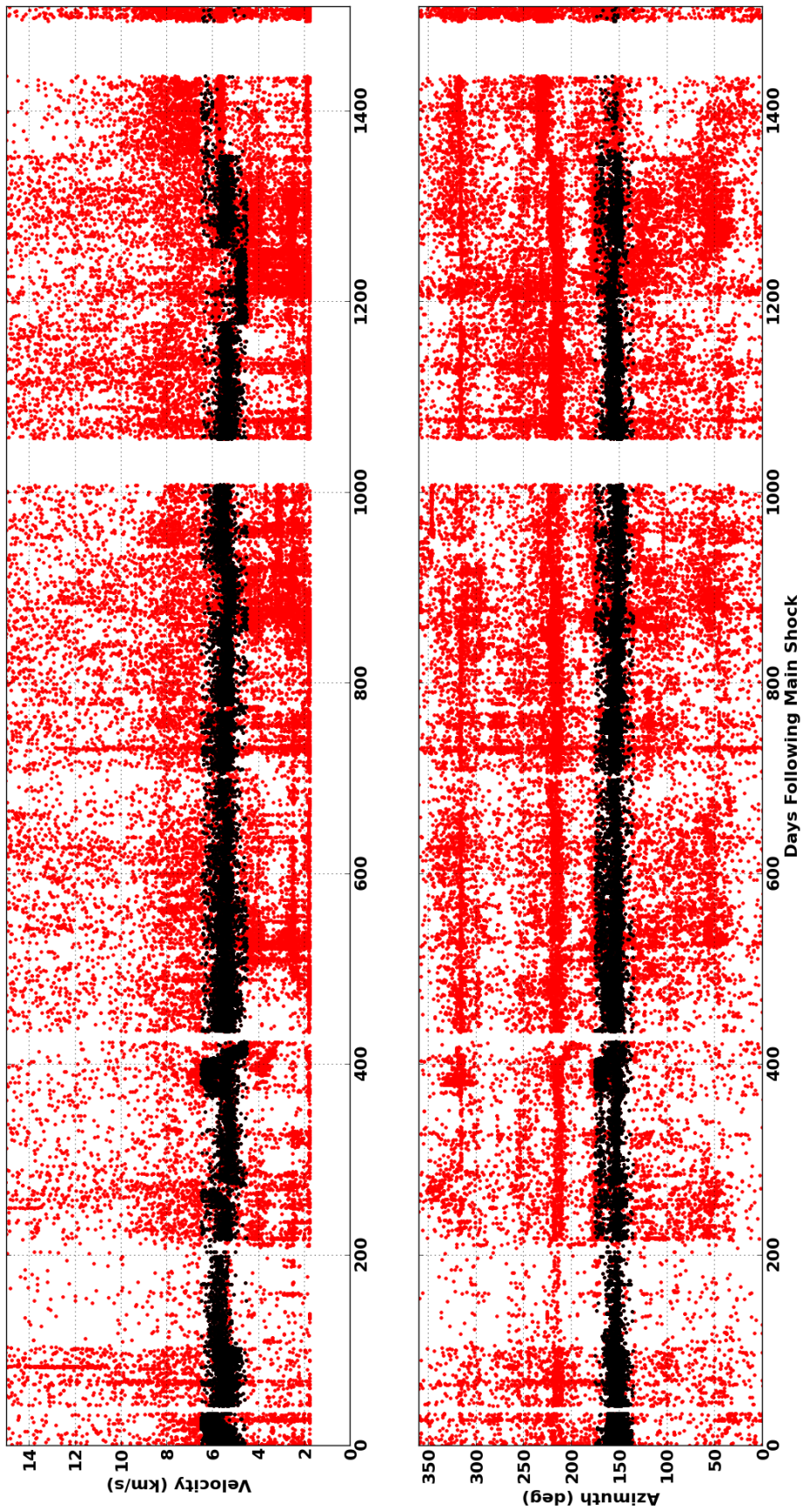

Fig. 3: FK measurements for framework detections, where the top plot is velocity, bottom plot is back azimuth, red dots show all detections, and black dots denote detections that passed the screening criteria. The x-axis denotes the number of days after the start of the sequence (21 February 2008). Gaps in detection processing are observed near days 5, 410, 1010, and 1450.

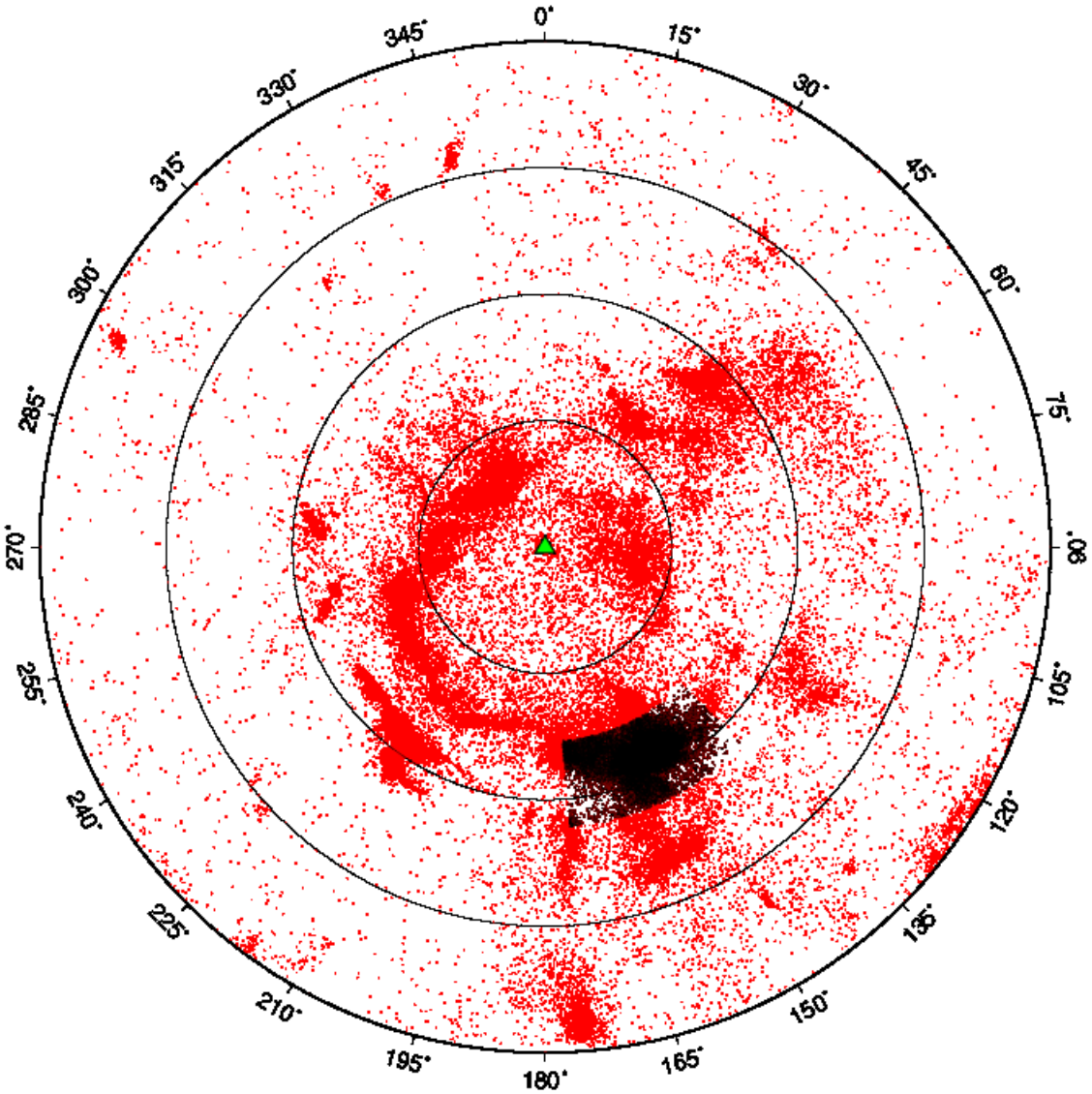

Fig. 4: Azimuth and slowness measurements for all accepted framework detections, where red shows all detections, black are those that passed the FK screening criteria, and the distance between concentric circles is 0.1 s/km, where the value for the inner most ring is 0.1 s/km.

3.3 Space-Time Distribution of Events

Figure 9 shows the relative relocation catalog from Pirli et al. (2013) and combined moment tensor solutions from Pirli et al. (2013) and Junek et al. (2014) colored as a function of days following the main shock. The figure shows the events are migrating across the rupture zone over time. Magenta events occur during the early stages of the sequence between days 0 and 100. Blue and cyan events tend to occur to the south of the magenta events between days 100 and 800. Green are located to the southeast of the blue and cyan events and occur between days 800 and 1100. Events occurring between days 1100 and 1400 are located to the north of the magenta events. Orange and red events tend to be located in the central area of the sequence. The moment tensor solutions show a preference for normal faulting along the western flank of the sequence and a mixture of strike-slip and oblique-normal faulting along its eastern edge.

Figures 10(a) and 10(b) show a time series of event detections per day following the main shock for the framework and NORSAR Analyst Reviewed Regional catalogs. The occurrence time of events with focal mechanisms or mb_{rel} greater than 4.0 are shown in the top section of Figure 10(a) and are color coded as a function of days following the mainshock. Figure 10(a) shows more events occurring in Storfjorden than documented in the NORSAR Analyst Reviewed Regional catalog. The framework is providing a higher fidelity catalog of events per day, which is highlight-

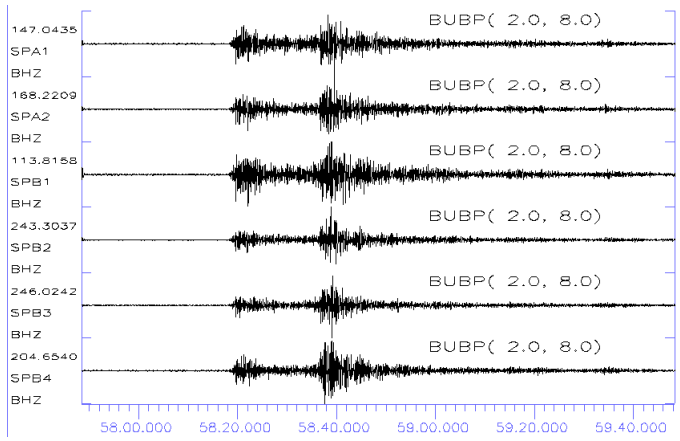

(a) Example 1: Valid signal detection.

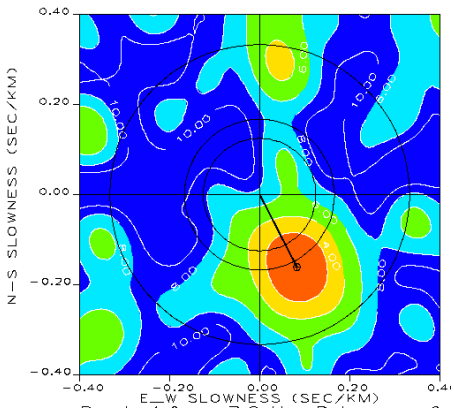

(b) Example 1: Correct azimuth and slowness.

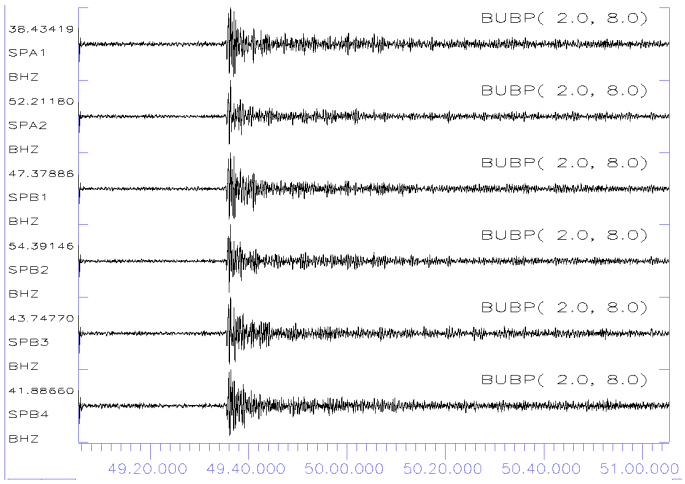

(c) Example 2: Valid signal detection.

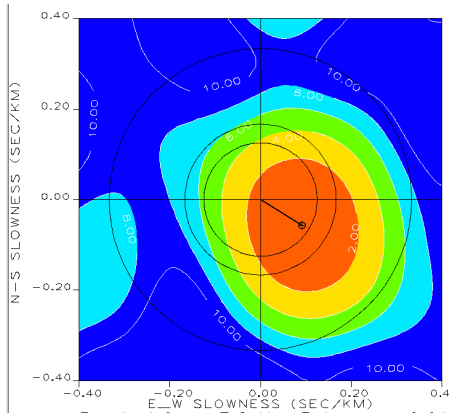

(d) Example 2: Incorrect azimuth and slowness.

Fig. 5: Examples of ESD detections and corresponding FK measurements for valid and invalid events.

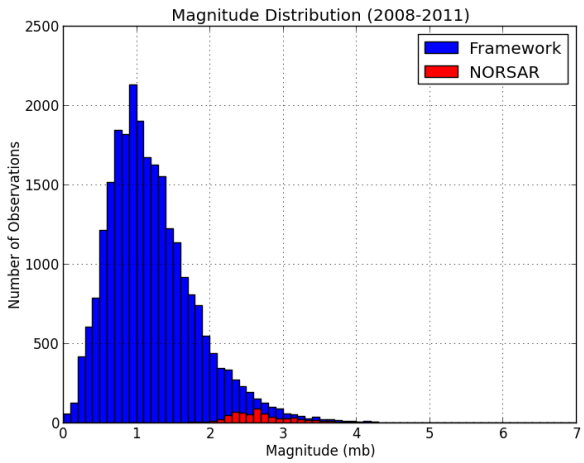

Fig. 6: Binned FMD for framework (blue) and NORSAR (red) catalogs.

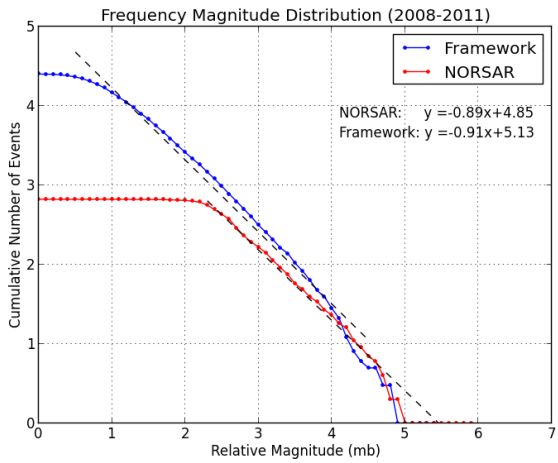

Fig. 7: Cumulative FMD for framework (blue) and NORSAR (red) catalogs

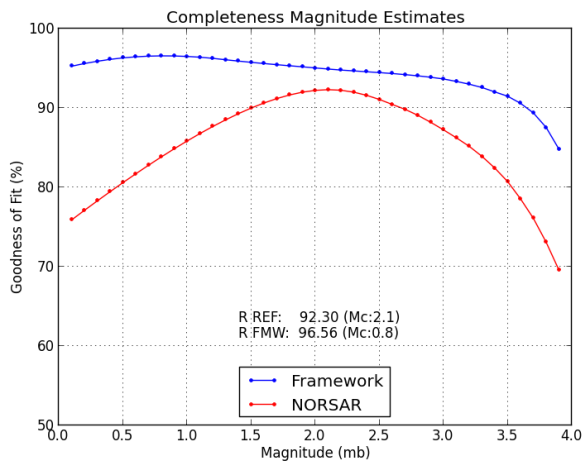

Fig. 8: Goodness of fit measurements for the linear portion of the modeled and observed frequency magnitude distributions for the framework (blue) and NORSAR (red) catalogs.

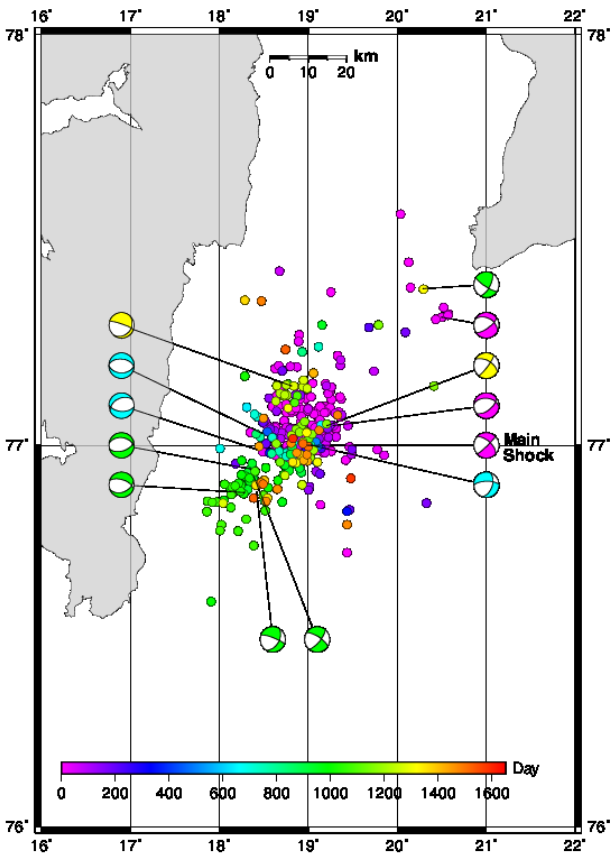

Fig. 9: Relative relocation catalog occurrence time color coded as a function of days following the main shock.

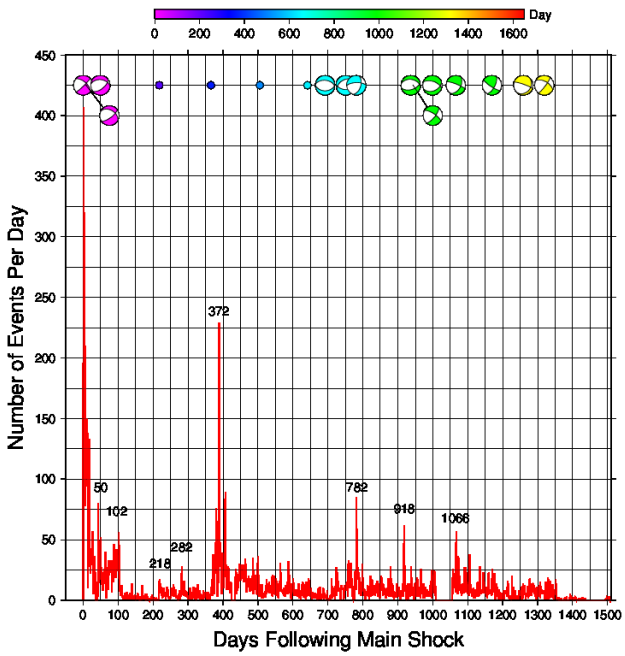

(a) Framework Catalog

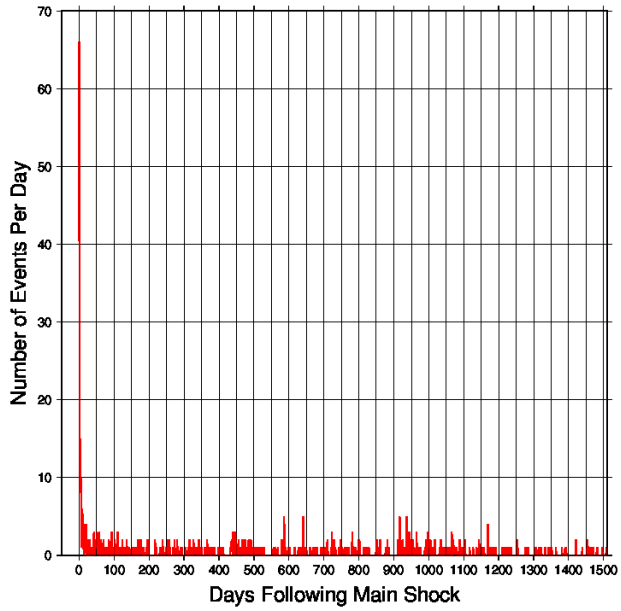

(b) NORSAR Analyst Reviewed Regional Catalog

Fig. 10: Detected events per day. a) Framework catalog after applying FK screening parameters, where focal mechanisms are color coded as a function of days following the main shock and numbers correspond to days displaying heightened branch activity. b) NORSAR Analyst Reviewed Regional catalog for Storfjorden.

ing at least eight branches (occurring on days 50, 102, 218, 282, 372, 782, 918, and 1066) that are not shown in the analyst reviewed bulletin. Unsurprisingly, several of these episodes coincide with the occurrence of large events shown in the top portion of Figure 10(a).

The initiation day, lifespan, and number of members in each event cluster (i.e., detections sharing the same detector ID) are shown in Figure 11. Lifespan bars indicate the rate of cluster generation is greatest at the beginning of the sequence and remains relatively constant until day 100. At this point, the cluster generation rate decreases and spikes on days when different branches are initiated. The lifespan of the clusters vary dramatically, where some last hours and others last the entire length of the sequence. The number of events constituting each cluster also varies significantly. Some groups have a single member, while others have 10 to 85 members.

Day 100 marks an interesting transition point in the sequence's evolution. Note in Figure 9 that all events occurring before day 100 (shown in magenta) are located in the NE section of the sequence. Between days 50 and 100, Figure 10(a) shows the number of events per day are increasing. After day 100, the sequence begins to migrate to the SW, the number of events per day drops below 25, and the cluster generation rate becomes near linear, where its slope (m) is ≈ 0.9 clusters/day. One possible explanation for this change in behavior is an asparity failure that allows the stress to propagate to the SW sections of the fault.

3.4 Inferring Tectonic Structure

Framework detections were matched to events in the relative relocation catalog based on origin time. After a single event match was found, all occurrences of the event's detector ID in the database were counted and the total represents the number of similar events detected throughout the sequence. In this study, we defined an event cluster as a group of framework detections that share a similar detector ID. Here, a total of 767 matches were found, which represents approximately 4.8% of all framework detections. All event clusters matched to events in the relative relocation catalog have well defined waveforms, whose S-P times are consistent with Storfjorden events. Selected examples of waveform segments for matched event clusters are shown in Figures 12(a) and 12(b).

Figure 13 shows event clusters with three or more members, relative to all events in the relative relocation catalog. The event activity plot (Figure 13(a)) highlights areas of heightened activity within the sequence. Moment tensor solutions show at least two different structures within the rupture zone: a linear feature trending NE-SW with oblique-normal to strike-slip faulting, and normal faults trending E-W. The NE-SW trending linear feature is illuminated by the green, red, blue, and magenta dots in the southeastern portion of the sequence. The orientation of this feature is consistent with the shear zone suggested by Bergh & Grogan (2003). A dashed black line shows the inferred extension of the shear zone through the sequence rupture zone. The end point is based on the location of the far northeastern clusters, which may be caused by stress build up at the fault termination point. It should be noted that approximately 95% of framework detections could not be linked to an event in the relative relocation catalog and are not shown in Figure 13.

Spatial occurrence time (day event occurred relative to main shock) statistics for events in each cluster are shown in Figures 13(b) and 13(c). The occurrence times for event clusters located near the main shock tend to be distributed throughout the sequence, where their average and standard deviation is approximately 600 days and 300 days. However, event clusters originating in the southwestern and northeastern sections of the sequence have narrower time distributions that follow its spatial migration over time. Figure 14 shows the time distribution of events in the most active cluster (shown in red in Figure 13(a)). Activity within this group peaks early in the sequence, decays steadily over the next 650 days, experiences moderate reactivation on day 700, and steadily decays again over the remainder of the sequence. This collection of correlated events are most likely produced by asperities or the release of residual stress in the area close to the epicenter of the main shock, and constitutes its own branch within the sequence.

4 Conclusions

We have demonstrated the use of an autonomous event detection and grouping system for studying aftershock sequence properties and inferring tectonic structure in situations where the deployment of temporary sensors is impractical. In this study, the automated system was able to exploit data from a permanent seismic array in the region and improved the catalog M_c by 1.3 magnitude units relative to the NORSAR regional reviewed catalog for Storfjorden.

Processing results generated for the 2008 Storfjorden aftershock sequence identified numerous events that were previously unknown. The results show the sequence is more complex than previous results suggest. New event clusters with varying duration and number of members were being generated at varying rates throughout the sequence. The spatiotemporal distribution of events was more consistent with an epidemic type aftershock (ETAS) model as opposed to the smooth exponential decay predicted by Omori's law (Ogata, 1988). The ETAS model suggests aftershocks continuously trigger smaller aftershock sequences over time in a manner similar to the spread of disease epidemics. Branching activity within the fault zone was highlighted by the reduced

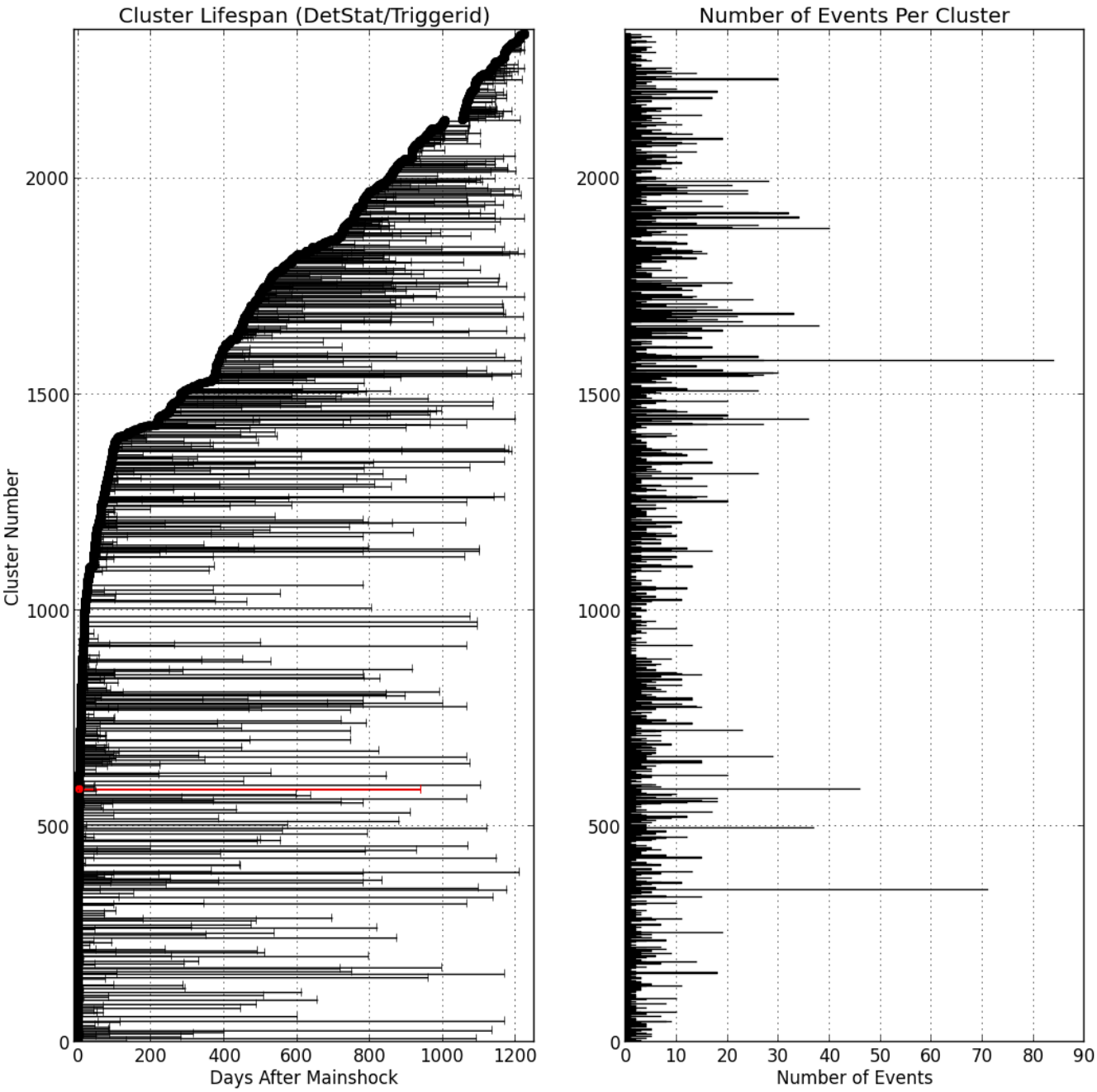

Fig. 11: Cluster lifespan (left panel) and number of events per cluster (right panel), where each point on the lifespan bars represents the initiation time of the cluster. The red bar highlights the most active cluster that contains a match to an event in the relative relocation catalog.

M_c achieved by the ESDs. This level of branching was not observable in the analyst reviewed catalog.

We were able to infer additional information about the tectonic structure within the fjord that was not obvious in the relative relocation or NORSAR analyst reviewed catalogs. Active event clusters were used to highlight areas of elevated activity within the fault zone. This information, combined with the relative relocation catalog, moment tensor solutions, and previously mapped tectonic features, allowed us to infer an extension to the previously mapped Tertiary shear zone through the fjord. Extension of the structure described by Bergh & Grogan (2003), now exhibiting oblique-slip behavior, and secondary activations of nearby E-W normal faults are the likely source of the sequence. This conclusion is supported by the orientation of the relative relocation

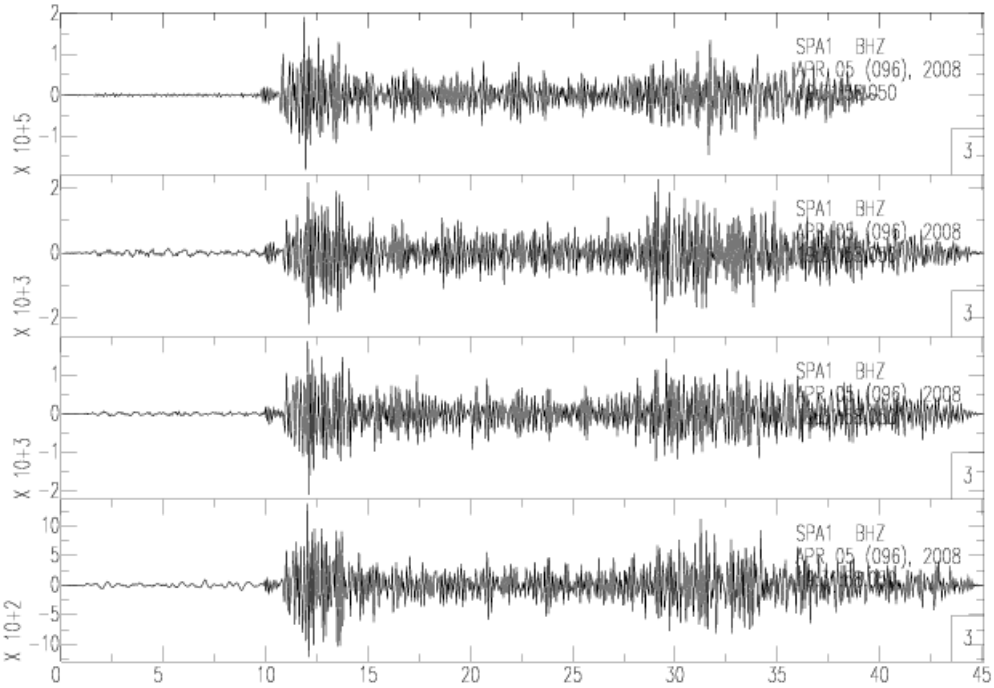

(a) Example 1

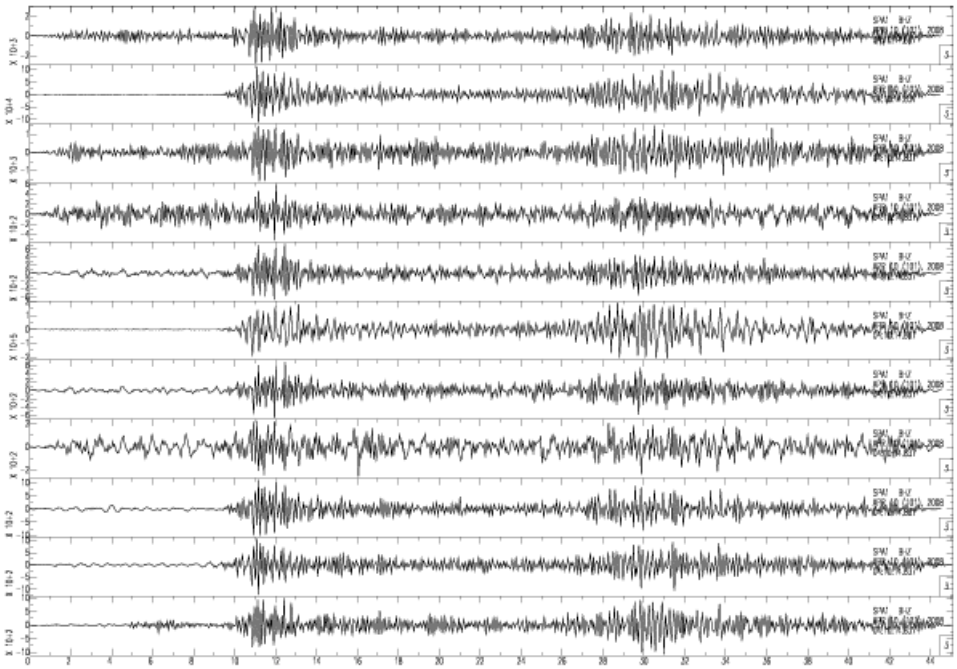

(b) Example 2

Fig. 12: Examples of waveforms from event clusters that match an event in the relative relocation catalog. Note the strong similarity among the first packet of the compressional wave, and the S-P times.

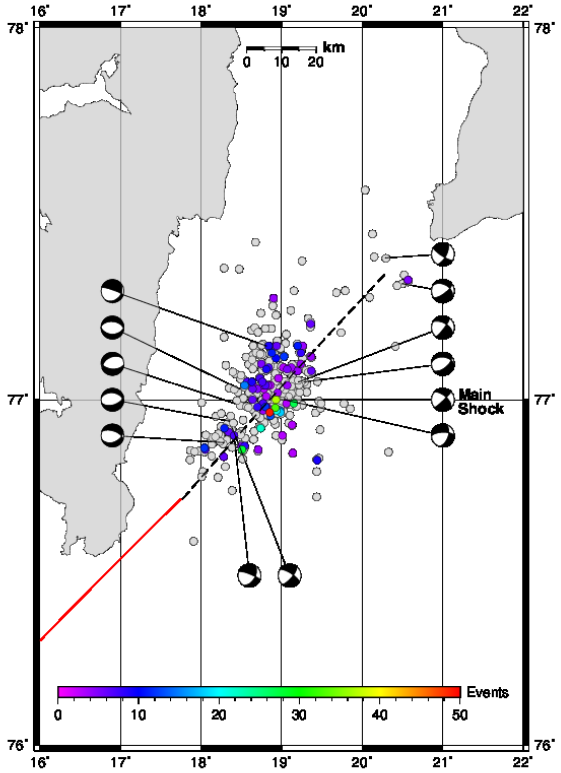

(a) Number of events per cluster

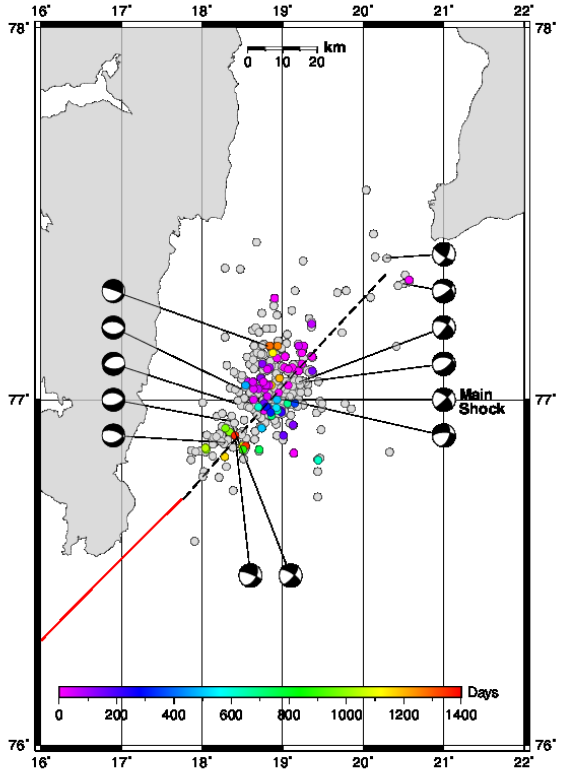

(b) Average event occurrence time per cluster

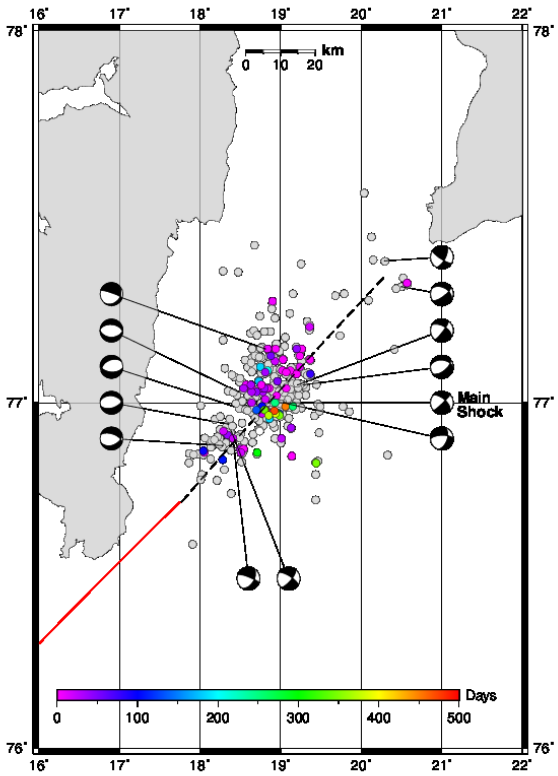

(c) Standard deviation of occurrence time per cluster

Fig. 13: Framework event cluster with more than 3 members matched to events in the relative relocation catalog, where the red line shows the location of the previously mapped Tertiary shear zone and the black dashed line represents the inferred location through the sequence rupture zone. Colored dots represent events clusters that are matched to an event in the relative relocation catalog and gray dots are unmatched events. a) Number of events per cluster. b) Average occurrence time of events per cluster. c) Standard deviation of occurrence time per cluster.

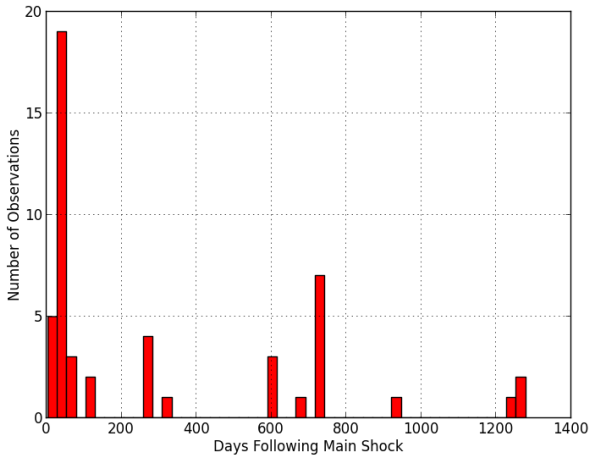

Fig. 14: Number of events per day associated to the most active event cluster, totaling 43 events. This clusters location in Figure 11 is shown by the red lifespan bar.

catalog and mixture of oblique-slip, strike-slip, and normal focal mechanisms.

Future work will focus on the application of ESDs to larger sequences (e.g., 2008 Sichuan sequence) for extending available datasets and inferring tectonic structure. In addition, the framework will be used to study the space-time distribution of selected aftershock sequences to determine their agreement with ETAS models.

Acknowledgements The plots shown in this paper were generated using the Generic Mapping Tools and Python via Matplotlib (Wessel & Smith, 1998; Hunter, 2007). The results presented in this paper are solely the opinion of the authors; they do not represent the official position or policy of the United States Government.

A Definition of FK Power

The FK_{pow} metric is a measure of multichannel coherence (i.e., semblance) and is defined as

$$FK_{pow} = \frac{\sum_{j=k-\frac{1}{2}N}^{k+\frac{1}{2}N} \left[\sum_{i=1}^{M} f_{i,j} \right]^2}{\frac{1}{M} \sum_{j=k-\frac{1}{2}N}^{k+\frac{1}{2}N} \left[\sum_{i=1}^{M} (f_{i,j})^2 \right]} \tag{3}$$

where M is the number of channels, N is the window length, k is the point where the window is centered, and $f_{i,j}$ is the ith sample value of the jth trace (Sheriff, 1973).

References

Bergh, S. G., & Grogan, P. (2003). Tertiary structure of the Sorkapp-Hornsund region, South Spitsbergen, and implication for the offshore southern extension of the fold-thrust belt. *Norwegian Journal of Geology*, (83), 43–60.

Gibbons, S. J., & Ringdal, F. (2006). The detection of low magnitude seismic events using array-based waveform correlation. *Geophysical Journal International*, *165*(1), 149–166.

Gutenberg, R., & Richter, C. F. (1944). Frequency of earthquake in California. *Bulletin of the Seismological Society of America*, *34*, 185–188.

Harris, D. B. (2006). Subspace detectors: Theory. No. ucrl-tr-222758, Lawrence Livermore National Laboratory.

Harris, D. B., & Dodge, D. A. (2011). An autonomous system for grouping events in a developing aftershock sequence. *Bulletin of the Seismological Society of America*, *101*(2), 763–774.

Hunter, J. D. (2007). Matplotlib: A 2d graphics environment. *Computing In Science & Engineering*, *9*(3), 90–95.

Junek, W. N., Harris, D. B., Ichinose, G. A., & Woods, M. T. (2008). Automated analysis of the Mogul-Somersett earthquake sequence. In *Eos Trans. American Geophysical Union, 89(53), Fall Meeting Supplement, abstract S51C-1756*.

Junek, W. N., Roman-Nieves, J., & Woods, M. T. (2014). Tectonic implications of earthquake mechanisms in Svalbard. *Geophysical Journal International*, *196*, 1152–1161.

Ogata, Y. (1988). Statistical models of earthquake occurrences and residual analysis for point processes. *Journal of the American Statistical Association*, *83*(401), 9–27.

Pirli, M., Schweitzer, J., & Paulsen, B. (2013). The Storfjorden, Svalbard, 2008-2012 aftershock sequence: Seismotectonics in a polar environment. *Tectonophysics*, (601), 192–205.

Schaff, D. P., & Waldhauser, F. (2010). One magnitude unit reduction in detection threshold by cross correlation applied to Parkfield (California) and China seismicity. *Bulletin of the Seismological Society of America*, *100*(6), 3224–3238.

Sheriff, R. E. (1973). *Encyclopedic Dictionary of Exploration Geophysics*. Society of Exploration Geophysicists.

Slinkard, M. E., Carr, D. B., & Young, C. J. (2013). Applying waveform correlation to three aftershock sequences. *Bulletin of the Seismological Society of America*, *103*(2A), 675–693.

Wessel, S., & Smith, W. (1998). New, improved version of the generic mapping tool released. *EOS Transactions AGU*, *79*, 579.

Wiemer, S., & Wyss, M. (2000). Minimum magnitude of completeness in earthquake catalogs: Examples from Alaska, the Western United States, Japan. *Bulletin of the Seismological Society of America*, *90*(4), 859–869.